Volume-averaged continuum approach for turbulent flows in porous media: An a-priori DNS analysis

By S. V. Apte†, X. He† AND B. D. Wood‡

The method of volume averaging is used to obtain upscaled continuum balance equations for turbulent flows. The volume-averaged equations give rise to an unclosed subgrid scale stress term, similar to large-eddy simulation (LES) equations, and an additional surface drag term that needs to be modeled. The unclosed terms are evaluated using *a-priori* analysis of direct numerical simulation (DNS) data for pore-scale turbulence in a face-centered cubic lattice at three different pore Reynolds numbers (300, 500, and 1000). The DNS data are used to assess the presence of any macroscale turbulence structures that are larger than the pore size. A standard closure model based on a modified Ergun equation, applicable to a wide range of Reynolds numbers covering Darcy to inertial flow regime, is evaluated for turbulent flows using the DNS data.

1. Introduction

The pressure-velocity relationships in porous media (known as Ergun–Forchheimer equations) have been known empirically for more than 100 years. Contrary to conventional thought about fluid flow in porous media, the inertial contribution to the flow field is often important in both engineering and natural applications, and the inertial terms can dramatically change the topology of the flow field (such as formation of jets, vortices, dead zones, etc., within pores). However, the mechanisms of how inertial and turbulent flows affect the large-scale friction factor are poorly understood (Hlushkou & Tallarek 2006). There are very few detailed particle image velocimetry (PIV) or DNS data on pore-scale characterization to develop upscaled models.

Furthermore, nearly all theoretical studies of dispersion in porous media have been for either (i) Stokes flow (which neglects the influence of inertial contributions completely) or (ii) inertial flow without any turbulence effects. Researchers typically rely on established empirical correlations for predicting transport and dispersive properties of flow in fixed beds and ultimately in reactor design (Eigenberger & Ruppel 2012). Development of Reynolds-averaged Navier-Stokes (RANS) models for flow at the pore-scale level has been attempted by numerous researchers. For example, the RANS $k-\epsilon$ model has been derived by time averaging the volume-averaged extended Darcy-Forchheimer model equations (Antohe & Lage 1997), by volume averaging the time-averaged Reynolds-averaged equation (Suga 2016), or by the double-decomposition technique developed based on exchangeability of volume-time or time-volume averaging (Pedras & De Lemos 2001). In these models, extra terms requiring closure are obtained by conducting numerical experiments on simple geometries such as a periodic array of rods and by using standard

† School of Mechanical, Industrial, and Manufacturing Engineering, Oregon State University
‡ School of Chemical, Biological, and Environmental Engineering, Oregon State University

turbulence closure techniques based on a gradient diffusion hypothesis. However, these models lack validation with experimental or DNS data.

In this work, we apply the method of volume averaging (MVA) to obtain the continuum, upscaled momentum balance equations for inertial and turbulent flows in porous media. The volume-averaged equations give rise to unclosed terms similar to a Reynolds stress in large-eddy simulation as well as to a surface drag term that needs to be modeled. A data set obtained from pore-scale, direct numerical simulations of turbulent flows in homogeneous porous media is used to evaluate closure models. Specifically, we investigate two research topics related to turbulence modeling in porous media: (i) Can one obtain macroscopic flow structures larger than the pore scale in turbulent flows through porous media at low porosity and (ii) do the empirically obtained coefficients of the modified Ergun correlation apply to the transitional and fully developed turbulent flows at high pore Reynolds numbers? The proposed developments are significant to a wide range of industrial and environmental applications, from the performance of packed bed reactors (Bernard & Wilhelm 1950) to subsurface groundwater remediation (Dagan 1984), environmental flows such as rivers over porous beds, and noise reduction in aircrafts using porous trailing edges of wings (Herr & Dobrzynski 2005).

The paper is arranged as follows. The volume-averaged continuum equations and the related closure model are described in Section 2. A triply periodic, homogeneous computational geometry and the numerical approach for pore-scale simulations of turbulent flow are provided in Section 3. Section 4 presents the turbulent statistics, obtained from the direct numerical simulations, such as the turbulence length scales, auto-correlations, and energy spectra. In addition, volume averaging of the DNS data set is used to evaluate the closure terms and closure models for different Reynolds numbers. Finally, Section 5 summarizes the results.

2. Volume-averaged continuum approach

Figure 1 shows a schematic of a representative elementary volume (REV) over which averaging is performed to derive the continuum volume-averaged Navier-Stokes (VANS) equations. To obtain meaningful VANS equations, it is assumed that the equivalent length scales associated with the pore size is much smaller than the length scale associated with the REV, which in turn is much smaller than the global length scale of the porous medium. In addition, variations in porosity averaged over the REV are considered negligible. Here, $\mathscr{V}(\mathbf{X})$ is the averaging domain, where $\mathbf{X}$ is its centroid, γ represents the fluid phase, κ the solid phase, $\mathscr{A}_{\gamma\kappa}(\mathbf{X})$ the interface between the two phases, and $\langle\rangle$ the volume averaging operator. The volume averaging of any quantity ψ in the fluid (γ) phase can then be written as

$$\langle\psi_\gamma\rangle = \frac{1}{V}\int_{\mathbf{r}\in\mathscr{V}(\mathbf{X})} I_\gamma(\mathbf{r})\psi(\mathbf{r})dV(\mathbf{r}), \tag{2.1}$$

where V is the total volume in the averaging domain and $I_\gamma(\mathbf{r})$ is the indicator function defined as

$$I_\gamma(\mathbf{r}) = \begin{cases} 1, & \mathbf{r}\in\mathscr{V}_\gamma. \\ 0, & \mathbf{r}\in\mathscr{V}_\kappa. \end{cases} \tag{2.2}$$

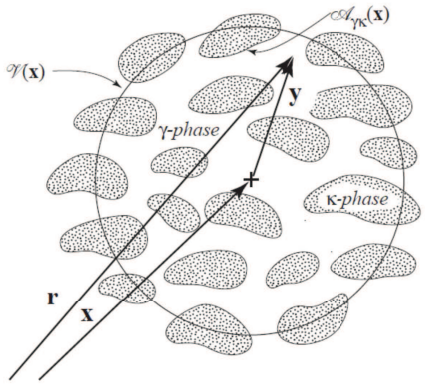

FIGURE 1. Schematic of the averaging volume over the solid and the fluid phase in a porous medium (Whitaker 1996).

The intrinsic average quantity is defined in a similar fashion except that the averaging volume used is the volume of a particular phase,

$$\langle\psi_\gamma\rangle^\gamma = \frac{1}{V_\gamma}\int_{\mathbf{r}\in\mathscr{V}(\mathbf{X})} I_\gamma(\mathbf{r})\psi(\mathbf{r})dV(\mathbf{r}). \tag{2.3}$$

As a result, the superficial averaged quantity $\langle\psi_\gamma\rangle$ can be related with the intrinsic averaged quantity $\langle\psi_\gamma\rangle^\gamma$ as

$$\langle\psi_\gamma\rangle = \varepsilon_\gamma\langle\psi_\gamma\rangle^\gamma, \tag{2.4}$$

where ε_γ is the porosity of the medium, defined as the ratio of the void volume (V_{void}) to the total volume (V_{total}).

In addition, Whitaker (1996) used the spatial averaging theorem and provided a relationship between the volume-averaged spatial derivative and the spatial derivative of the volume-averaged quantity as

$$\langle\nabla\psi_\gamma(\mathbf{r})\rangle = \nabla\langle\psi_\gamma\rangle + \frac{1}{V}\int_{\mathbf{r}\in\mathscr{A}_{\gamma\kappa}(\mathbf{X})}\mathbf{n}_{\gamma\kappa}(\mathbf{r})\psi_\gamma(\mathbf{r})dA(\mathbf{r}). \tag{2.5}$$

The volume averaging procedure can be applied to the continuity and momentum equations for an incompressible fluid, using $\widetilde{\boldsymbol{u}}_\gamma$ and $\widetilde{p}_\gamma$ as the spatial fluctuation velocity and pressure, defined as

$$\widetilde{\boldsymbol{u}}_\gamma = \boldsymbol{u}_\gamma - \langle\boldsymbol{u}_\gamma\rangle^\gamma, \quad \widetilde{p}_\gamma = p_\gamma - \langle p_\gamma\rangle^\gamma. \tag{2.6}$$

With this method, the volume-averaged continuum equations for stationary porous medium with homogeneous porosities are obtained as (Whitaker 1996)

$$\epsilon_\gamma\nabla\cdot\langle\boldsymbol{u}_\gamma\rangle^\gamma = 0, \tag{2.7}$$

$$\begin{aligned}\rho_\gamma\frac{\partial\langle\boldsymbol{u}_\gamma\rangle^\gamma}{\partial t} + \rho_\gamma\langle\boldsymbol{u}_\gamma\rangle^\gamma\cdot\nabla\langle\boldsymbol{u}_\gamma\rangle^\gamma + \underbrace{\rho_\gamma\varepsilon_\gamma^{-1}\nabla\cdot\langle\widetilde{\boldsymbol{u}}_\gamma\otimes\widetilde{\boldsymbol{u}}_\gamma\rangle}_{\text{volume filter closure}} = \\ -\nabla\langle p_\gamma\rangle^\gamma + \rho_\gamma\mathbf{g} + \mu_\gamma\nabla^{\mathbf{2}}\langle\boldsymbol{u}_\gamma\rangle^\gamma + \underbrace{\frac{1}{V_\gamma}\int_{\mathcal{A}_{\gamma\kappa}}\mathbf{n}_{\gamma\kappa}\cdot(-\mathbf{I}\widetilde{p}_\gamma + \mu_\gamma\nabla\otimes\widetilde{\boldsymbol{u}}_\gamma)\mathbf{d}A}_{\text{surface filter closure}}.\end{aligned} \tag{2.8}$$

Here ρ_γ is the fluid density and μ_γ the dynamic viscosity, respectively. Because of the non-linear inertial terms and volume averaging across the fluid-solid boundary, two unclosed terms identified as the volume filter closure and surface filter closure are obtained that need to be modeled. The volume filter term represents a standard Reynolds stress term, and the surface term is a drag term owing to integrated pressure and viscous forces on embedded boundaries within the filter volume. The volume filter term can be modeled similarly to the Reynolds stress in a large-eddy simulation approach and using the Boussinesq hypothesis of gradient diffusion.

For stationary flows in a triply periodic, homogeneous porous medium, the above equations can be greatly simplified. Gradients of the volume-averaged velocity disappear, and thus the volume filter term modeled using the gradient diffusion hypothesis drops out, giving

$$0 = -\nabla\langle p_\gamma\rangle^\gamma + \frac{1}{V_\gamma}\int_{\mathcal{A}_{\gamma\kappa}} \mathbf{n}_{\gamma\kappa}\cdot(-\mathbf{I}\widetilde{p}_\gamma + \mu_\gamma\nabla\otimes\widetilde{\boldsymbol{u}}_\gamma)\,\mathbf{d}A. \tag{2.9}$$

Here the gravity term is neglected, or it can be absorbed in the volume-averaged mean pressure gradient term. The surface viscous drag term on the right side also drops out for the homogeneous flow; it is retained here simply for completeness of the drag term. As shown by Whitaker (1996) using theoretical analysis, the surface drag term can be expressed in terms of an effective permeability,

$$\frac{1}{V_\gamma}\int_{\mathcal{A}_{\gamma\kappa}} \mathbf{n}_{\gamma\kappa}\cdot(-\mathbf{I}\widetilde{p}_\gamma + \mu_\gamma\nabla\otimes\widetilde{\boldsymbol{u}}_\gamma)\mathbf{d}A = -\mu_\gamma\mathbf{K}_{\text{eff}}^{-1}\varepsilon_\gamma\langle\boldsymbol{u}_\gamma\rangle^\gamma = -\mu_\gamma\mathbf{K}_{\text{eff}}^{-1}\langle\boldsymbol{u}_\gamma\rangle, \tag{2.10}$$

where $\mathbf{K}_{\text{eff}}$ is the effective permeability tensor and $\langle\boldsymbol{u}_\gamma\rangle$ is the superficial velocity. The effective permeability tensor is generally expressed as

$$\mathbf{K}_{\text{eff}}^{-1} = \mathbf{K}^{-1}\left(\mathbf{I}+\mathbf{F}\right), \tag{2.11}$$

where $\mathbf{K}$ and $\mathbf{F}$ are the permeability and Forchheimer tensor, respectively.

In the limit of Stokes flow, the drag term depends only on the permeability tensor, whereas the inertial effects are important at higher pore Reynolds numbers such that the Forchheimer correction becomes dominant. The permeability tensor depends only on the geometry of the porous medium, but the Forchheimer tensor can depend on the pore Reynolds number, the orientation of the beads relative to the direction of the volume-averaged flow and pressure gradient, as well as other geometric parameters. Universally valid expressions for these tensors have not been successfully developed. They are determined empirically through substantial experimental data and numerical simulations in the Stokes and steady or unsteady laminar regimes. A widely used expression for drag force is the Ergun equation, which can be written using the permeability and Forchheimer tensors as

$$\mathbf{K} = \frac{d_p^2\varepsilon_\gamma^3}{\mathcal{A}(1-\varepsilon_\gamma)^2}\mathbf{I}, \quad \mathbf{F} = \tilde{F}|\langle\boldsymbol{u}_\gamma\rangle^\gamma|\mathbf{I}, \quad \tilde{F} = \frac{\varepsilon_\gamma}{\mathcal{B}(1-\varepsilon_\gamma)}\frac{d_p}{\nu_\gamma}, \tag{2.12}$$

where $d_p = 6V_\kappa/A_{\gamma\kappa}$ is the effective diameter of the solid beads with V_κ their volume and $A_{\kappa\gamma}$ the surface area. Several different values have been proposed for the model coefficients $\mathcal{A}$ and $\mathcal{B}$ (Bird *et al.* 2002; Macdonald *et al.* 1979; Breugem *et al.* 2006; Bǎgci *et al.* 2014). Bǎgci *et al.* (2014) obtained experimental data on a wide range of Reynolds numbers with steel spheres of two different diameters and fitted the data with $\mathcal{A} = 150$ and $\mathcal{A}/\mathcal{B} = 1.0$–$1.75$. Macdonald *et al.* (1979) used experimental and computational data in which particle sizes, porosity, and pore Reynolds numbers were varied and proposed using $\mathcal{A} = 180$ and $\mathcal{A}/\mathcal{B} = 1.8$–$4$ as well as replacing ε_γ^3 by $\varepsilon_\gamma^{3.6}$. One of the main objectives

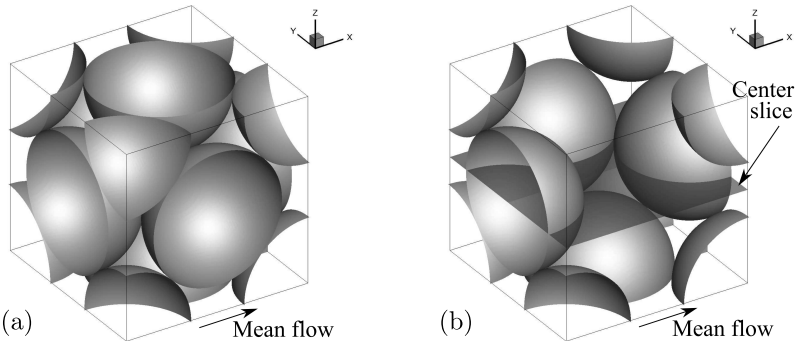

FIGURE 2. Face-centered cubic porous unit cell: (a) full 3D geometry; (b) same as (a) except some beads are removed so that the flow region inside the unit cell can be observed.

of the present work is to generate a DNS data set for high pore Reynolds number (up to 1000) turbulent flows to investigate the predictive capability of the modified Ergun correlation in the fully turbulent regime.

3. Computational geometry and numerical approach

A porous face-centered cubic unit cell (Figure 2) was adopted for direct numerical simulation of turbulent flow. The domain has a half sphere entering at each face of a cube; a half of a quarter sphere is placed at each corner so that the entire domain is geometrically periodic. The face-centered cubic arrangement creates a highly tortuous structured packing with the lowest possible porosity ($\epsilon_\gamma = 0.26$). Due to the extreme compactness of the pore space, the flow through the unit cell experiences rapid expansion and contraction. To drive the flow through the porous media, a pressure gradient is imposed in x-direction and a triply periodic boundary condition is applied for the unit cell. A majority of flow enters the cubic cell through the upstream open corners, converges into the center pore resulting in strong accelerations and decelerations, and then leaves the unit cell along downstream corners. Following Hill & Koch (2002), we used a constant pressure gradient, whose magnitude is proportional to the non-dimensional body force, to drive the flow. Details on the computational setup, the body force used, the grid refinement study, and the mean and turbulence characteristics are described in our previous work (He *et al.* 2018). The present work investigates the flows at three different pore Reynolds numbers of 300, 500, and 1000. The pore Reynolds number, Re_p, is defined as

$$Re_p = \frac{\langle u_\gamma \rangle^\gamma D_B}{\nu_\gamma} \frac{\varepsilon_\gamma}{1 - \varepsilon_\gamma}, \tag{3.1}$$

where D_B is the bead diameter.

The numerical approach is based on a fictitious domain method to handle arbitrarily shaped immersed objects without requiring body-fitted grids (Apte *et al.* 2009). Uniform Cartesian grids are used in the entire simulation domain, including both fluid and solid phases. A rigidity constraint force is imposed inside the solid part to enforce rigid body motion and satisfy the no-slip boundary condition. The following governing equations are solved over the entire domain, including the regions within the solid bed. The rigidity

constraint force, $\boldsymbol{f}$, is applied, which is non-zero only in the solid region.

$$\nabla \cdot \boldsymbol{u} = 0, \tag{3.2}$$

$$\rho_\gamma \left[\frac{\partial \boldsymbol{u}}{\partial t} + (\boldsymbol{u} \cdot \nabla)\, \boldsymbol{u} \right] = -\nabla p + \mu_\gamma \nabla^2 \boldsymbol{u} + \rho_\gamma \boldsymbol{g} + \boldsymbol{f}\,. \tag{3.3}$$

Here, $\boldsymbol{u}$ is the velocity vector with components given by $\boldsymbol{u} = (u_x, u_y, u_z)$, ρ_γ is the fluid density, μ_γ the fluid dynamic viscosity, p the pressure, and $\boldsymbol{g}$ the gravitational acceleration. The details of the algorithm, as well as very detailed verification and validation studies, have been published elsewhere (Apte *et al.* 2009). A fully parallel, structured, collocated grid solver has been developed and thoroughly verified and validated for a range of test cases specific to porous media flows (Wood *et al.* 2015). The absence of highly skewed unstructured mesh at the bead surface has been shown to accelerate the convergence and lower the uncertainty for porous media simulations (Finn & Apte 2013).

4. Results

Direct numerical simulation of pore-scale turbulence was performed in a unit cell of a face-centered cubic lattice at three different pore Reynolds numbers (300, 500, and 1000). Adequacy of the computational domain size, Eulerian statistics of mean velocity and turbulent kinetic energy, spatial variances for instantaneous and temporal fluctuation velocities, and Lagrangian multiscale statistics have been analyzed and published by He *et al.* (2018). In the present work, we performed post-processing of the DNS data to obtain integral length scales, energy spectra, and volume-averaged flow data.

4.1. *Integral length scales and energy spectra*

An important question for inertial flows through porous media is whether the coherent structures observed on the pore scale remain confined to an individual pore (Evseev 2017) or can grow and extend to multiple pores (Agnaou *et al.* 2016). This can be best addressed for the turbulent flows by using the Eulerian two-point auto-correlations to compute the integral length scales and compare them to the characteristic pore size. The time-averaged Eulerian two-point auto-correlations were computed as

$$\rho_{ij}^E(|\boldsymbol{s}|) = \frac{\overline{\langle u_i'(\boldsymbol{x},t)\, u_j'(\boldsymbol{x}+\boldsymbol{s},t)\rangle}}{\overline{\langle u_i'(\boldsymbol{x},t)\, u_j'(\boldsymbol{x},t)\rangle}}. \tag{4.1}$$

Here, ρ_{ij}^E is the Eulerian auto-correlation and $\boldsymbol{s}$ represents the set of all possible vector displacements where the auto-correlation is calculated. The correlations were first computed at 100,000 randomly picked locations ($\boldsymbol{x}$) in the fluid domain at one instant of time and then spatially averaged. This procedure was repeated over 30 flow through times to remove any temporal variations in the spatially averaged auto-correlations.

In Figure 3(a), the auto-correlations with temporal fluctuating velocity component in x-direction are plotted against the position vector $|\boldsymbol{s}|$, nondimensionalized by the bead diameter D_B. The correlation near the origin drops off faster at higher Re_p, indicating that the flow decorrelates more rapidly with distance at high Reynolds numbers than at low Reynolds numbers. The Eulerian integral length scale, L_{11}^E, is calculated by integrating the correlations over the abscissa; the results are presented in Table 1. The integral length scales decrease with increasing Reynolds numbers. Moreover, even for the lowest Reynolds number flow, the integral length scale is only about 10% of the bead diameter, indicating that the coherent structures are confined within the pore. These

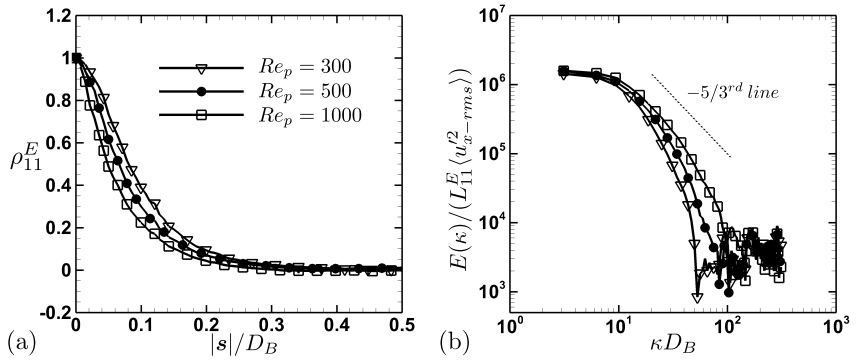

FIGURE 3. Turbulence statistics for different Reynolds numbers: (a) Eulerian auto-correlations; (b) energy spectra.

Re_p	300	500	1000
$\frac{L_{11}^E}{D_B}$	0.102	0.0884	0.0684

TABLE 1. Eulerian integral length scales normalized by the bead diameter.

results qualitatively agree with what was reported in Patil & Liburdy (2013), where a PIV measurement was carried out to determine the integral scales in different pores. Such observations support the pore scale prevalence hypothesis (PSPH) and the results reported by Jin *et al.* (2015), implying that the turbulence at the pore scale is strongly affected by the pore geometry. The tortuous paths within the porous bed break down the turbulence structures, and the presence of macroscopic turbulence structures that span multiple pores was not observed in the present low porosity configuration.

The energy spectra normalized by the integral length scale and the root-mean-square fluctuating velocity in x-direction are shown in Figure 3(b). The wavenumber κ is also scaled by the bead diameter, D_B. Distinct regions of $-5/3^{rd}$ law are not easily observed at the lower Reynolds numbers; however, a small region of inertial subrange with the $-5/3^{rd}$ law is observed especially for the highest Reynolds number.

4.2. *Volume averaging of the DNS data*

In order to verify the volume-averaged continuum model for turbulent flow through porous media, *a-priori* analysis of the DNS data set obtained for the three Reynolds numbers is conducted. The pressure drop through the porous medium was computed using DNS and compared with the experimental data of Băgci *et al.* (2014) for a wide range of Reynolds numbers covering the pre-Darcy, Darcy, laminar Forchheimer, and turbulent regimes. The data are also compared with the modified Ergun equation. Combining Eqs. (2.9)-(2.10) and (2.12), one can write an expression for the average pressure drop in the mean flow direction as

$$\frac{\Delta\langle p_\gamma\rangle^\gamma}{L} = \frac{\mu_\gamma}{K_{\text{eff}}}\langle u_\gamma\rangle = A\frac{(1-\varepsilon_\gamma)^2\mu_\gamma}{d_p^2\varepsilon_\gamma^3}\langle u_\gamma\rangle + B\frac{(1-\varepsilon_\gamma)\rho_\gamma}{d_p\varepsilon_\gamma^3}\langle u_\gamma\rangle^2, \tag{4.2}$$

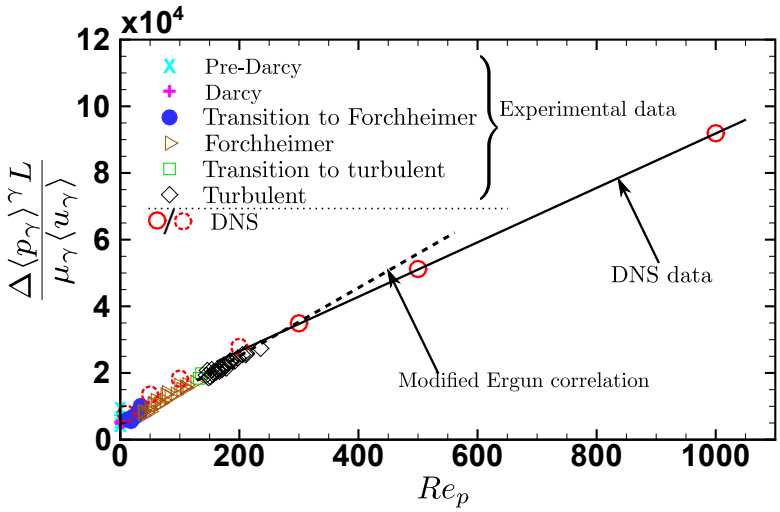

FIGURE 4. Normalized reduced pressure drop obtained from DNS for different Reynolds numbers compared with the experimental data of Băgci *et al.* (2014) and predictions using the modified Ergun correlation for the effective permeability.

where L is the length of the porous medium, $\Delta\langle p_\gamma\rangle^\gamma$ is the magnitude of the average pressure drop, $\langle u_\gamma\rangle$ is the component of the superficial velocity in the mean flow direction, and K_{eff} is the effective permeability in the mean flow direction. The first term on the right side can be used to describe the pre-Darcy and Darcy flow regimes, whereas the second term provides the Forchheimer correction for inertial regime. Note that the above modified Ergun correlation gives a quadratic relation between the pressure drop and the volume-averaged superficial velocity $\langle u_\gamma\rangle$.

The reduced pressure drop $\Delta\langle p_\gamma\rangle^\gamma/(L\langle u_\gamma\rangle)$ normalized by μ_γ/L^2 is plotted against the pore Reynolds number in Figure 4 together with the experimental data by Băgci *et al.* (2014) at lower Reynolds numbers. To validate the DNS results, four cases with lower pore Reynolds numbers of Re_p =10, 50, 100, and 200 are included in the figure as dashed circles and show reasonable agreement with experimental data. Small overprediction of the reduced pressure is observed, and this is potentially attributed to the fact that for low Re_p the inertial contribution to the hydraulic conductivity is small and it is solely determined by the geometry of the porous beads. The experimental data is for randomly packed porous media as opposed to present simulations for arranged FCC packing.

A straight line for the normalized reduced pressure in the high Re_p flows means that the pressure drop actually varies quadratically with the volume-averaged velocity. The coefficient B in the modified Ergun correlation [Eq. (4.2)] determines the slope of this line and is sensitive in various regimes of the flow. Using a curve fit to the experimental data, Băgci *et al.* (2014) obtained $A = 150$ and $B = 1.0$ for the turbulent regime. The value for coefficient B was lower for turbulent flows compared to the standard value of $B = 1.75$ in the Darcy and laminar Forchheimer regions. The volume-averaged superficial velocity is directly computed from the DNS data and is used to plot the normalized reduced pressure for higher Reynolds numbers investigated here. The DNS data also predict a straight line relation even in the fully turbulent regime; however, the slope of the line is lower than the proposed value of $B = 1.0$. More detailed investigations are

needed to understand the physics behind the predicted lower pressure drops in the highly turbulent regime.

5. Summary and conclusions

Direct numerical simulation (DNS) of pore-scale turbulence is performed in a unit cell of a face-centered cubic lattice at three different pore Reynolds numbers (300, 500, and 1000). The DNS data set is used to evaluate closure terms in upscaled continuum balance equations obtained by applying the method of volume averaging. The volume-averaged equations give rise to unclosed terms similar to a Reynolds stress in large-eddy simulation as well as a surface drag term that needs to be modeled. We evaluated a closure model based on a modified Ergun equation applicable to a wide range of Reynolds numbers that spans the Darcy and Forchheimer regimes for steady and unsteady inertial flows using *a-priori* analysis of the DNS data.

Firstly, the integral length scales were found to be less than 10% of the bead diameters for the present porous bed with very low porosity. The densely packed beads tend to break the turbulence structures, and the presence of macroscale flow structures larger than the pore scale was not found for the cases studied. Secondly, the averaged pressure drop was found to be a quadratic function of the volume-averaged velocity even in the highly turbulent regime. However, the empirically obtained coefficients of the modified Ergun correlation tend to overpredict the pressure drop in the fully turbulent flow regime. These findings should be further verified by investigating turbulent flows in randomly packed porous media as well as by investigating the weakly turbulent and steady/unsteady inertial regimes.

Acknowledgments

Sourabh Apte acknowledges hosts Sadaf Sobhani and Matthias Ihme, as well as Luca Brandt for useful discussions. Computational resources at PNNL's Cascade cluster are also acknowledged.

REFERENCES

Agnaou, M., Lasseux, D. & Ahmadi, A. 2016 From steady to unsteady laminar flow in model porous structures: an investigation of the first Hopf bifurcation. *Comput. Fluids* **136**, 67–82.

Antohe, B. V. & Lage, J. L. 1997 A general two-equation macroscopic turbulence model for incompressible flow in porous media. *Int. J. Heat Mass Transfer* **40**, 3013–3024.

Apte, S. V., Martin, M. & Patankar, N. A. 2009 A numerical method for fully resolved simulation (FRS) of rigid particle-flow interactions in complex flows. *J. Comput. Phys.* **228**, 2712–2738.

Bağci, O., Dukhan, N. & Ozdemir, M. 2014 Flow regimes in packed beds of spheres from pre-Darcy to turbulent. *Transport in Porous Media* **104**, 501–520.

Bernard, R. & Wilhelm, R. 1950 Turbulent diffusion in fixed beds of packed solids *Chem. Eng. Prog* **46**, 233–244.

Bird, R. B., Stewart, W. E. & Lightfoot, E. N. 2002 *Transport Phenomena*. John Wiley.

Breugem, W., Boersma, B. & Uittenbogaard, R. 2006 The influence of wall permeability on turbulent channel flow. *J. Fluid Mech.* **562**, 35–72.

Dagan, G. 1984 Solute transport in heterogeneous porous formations. *J. Fluid Mech.* **145**, 151–177.

Eigenberger, G. & Ruppel, W. 2012 *Catalytic Fixed-Bed Reactors*. Wiley Online Library.

Evseev, A. R. 2017 Visual study of turbulent filtration in porous media *J. Porous Media* **20**, 549–557.

Finn, J. & Apte, S. V. 2013 Relative performance of body fitted and fictitious domain simulations of flow through fixed packed beds of spheres. *Int. J. Multiphase Flow* **56**, 54–71.

He, X., Apte, SV., Schneider, K. & Kadoch, B. 2018 Angular multiscale statistics of turbulence in a porous bed. *Phys. Rev. Fluids* **3**, 084501.

Herr, M. & Dobrzynski, W. 2005 Experimental investigations in low-noise trailing edge design. *AIAA Journal* **43**, 1167–1175.

Hill, R. J. & Koch, D. L. 2002 The transition from steady to weakly turbulent flow in a close-packed ordered array of spheres. *J. Fluid Mech.* **465**, 59–97.

Hlushkou, D. & Tallarek, U. 2006 Transition from creeping via viscous-inertial to turbulent flow in fixed beds. *J. Chromatogr. A* **1126**, 70–85.

Jin, Y., Uth, M. F., Kuznetsov, A. V. & Herwig, H. 2015 Numerical investigation of the possibility of macroscopic turbulence in porous media: a direct numerical simulation study. *J. Fluid Mech.* **766**, 76–103.

Macdonald, I. F., El-Sayed, M. S., Mow, K & Dullien, F. A. L. 1979 Flow through porous media—the ergun equation revisited. *Ind. Eng. Chem. Fundam.* **18**, 199–208.

Patil, V. A. & Liburdy, J. A. 2013 Flow structures and their contribution to turbulent dispersion in a randomly packed porous bed based on particle image velocimetry measurements. *Phys. Fluids* **25**, 113303.

Pedras, M. H. J. & De Lemos, M. J. S. 2001 Macroscopic turbulence modeling for incompressible flow through undeformable porous media. *Int. J. Heat Mass Transfer* **44**, 1081-1093.

Suga, K. 2016 Understanding and modelling turbulence over and inside porous media. *Flow Turbul. Combust.* **96**, 717–756.

Whitaker, S. 1996 The Forchheimer equation: a theoretical development. *Transp. Porous Media* **25**, 27–61.

Wood, B. D., Apte, S. V., Liburdy, J. A., Ziazi, R. M., He, X., Finn, J. R. & Patil, V. A. 2015 A comparison of measured and modeled velocity fields for a laminar flow in a porous medium. *Adv. Water Resour.* **85**, 45–63.